Astroparticle Physics 62 (2015) 21–29

Contents lists available at ScienceDirect

Astroparticle Physics

journal homepage: www.elsevier.com/locate/astropart

Measurement of the radial density gradient of cosmic ray in the heliosphere by the GRAPES-3 experiment

H. Kojima [a,b], H.M. Antia [b,c], S.R. Dugad [b,c], S.K. Gupta [b,c,*], Y. Hayashi [b,d], P. Jagadeesan [b,c], A. Jain [b,c], S. Kawakami [b,d], P.K. Mohanty [b,c], T. Nonaka [b,d], A. Oshima [b,e], B.S. Rao [b,c], S. Shibata [b,e], The GRAPES-3 Collaboration

[a] Faculty of Engineering, Aichi Institute of Technology, Toyota City 470-0392, Japan
[b] The GRAPES-3 Experiment, Cosmic Ray Laboratory, Ooty 643 001, India
[c] Tata Institute of Fundamental Research, Mumbai 400 005, India
[d] Graduate School of Science, Osaka City University, Osaka 558-8585, Japan
[e] College of Engineering, Chubu University, Kasugai, Aichi 487-8501, Japan

ARTICLE INFO

Article history:
Received 24 April 2014
Received in revised form 13 June 2014
Accepted 2 July 2014
Available online 10 July 2014

Keywords:
Cosmic rays
Heliosphere
Solar wind
Convection
Diffusion

ABSTRACT

A radial anisotropy in the flux of cosmic rays in heliosphere was theoretically predicted by Parker and others within the framework of the diffusion–convection mechanism. The solar wind is responsible for sweeping out the galactic cosmic rays, creating a radial density gradient within the heliosphere. This gradient coupled with the interplanetary magnetic field induces a flow of charged particles perpendicular to the ecliptic plane which was measured and correctly explained by Swinson, and is hereafter referred as 'Swinson flow'. The large area GRAPES-3 tracking muon telescope offers a powerful probe to measure the Swinson flow and the underlying radial density gradient of the galactic cosmic rays at a relatively high rigidity of ~100 GV. The GRAPES-3 data collected over a period of six years (2000–2005) were analyzed and the amplitude of the Swinson flow was estimated to be (0.0644 ± 0.0008)% of cosmic ray flux which was an $\sim 80\sigma$ effect. The phase of the maximum flow was at a sidereal time of (17.70 ± 0.05) h which was 18 min earlier than the expected value of 18 h. This small 18 min phase difference had a significance of $\sim 6\sigma$ indicating the inherent precision of the GRAPES-3 measurement. The radial density gradient of the galactic cosmic rays at a median rigidity of 77 GV was found to be 0.65% AU^{-1}.

1. Introduction

The heliosphere comprises the region of space surrounding the Sun where the solar wind exerts sufficient pressure to sweep out the galactic cosmic rays into the interstellar medium. This region contains the interplanetary magnetic field (IMF) which is connected to the Sun, and is also frozen into the solar wind. The anchoring of the IMF to the solar surface and the flow of the solar wind forces the IMF outwards into a spiral form due to solar rotation. The solar wind results in the convection of charged particles away from the Sun, and well beyond the heliosphere lies the interstellar region where the galactic cosmic rays become largely isotropic. The random motion and the interactions of the galactic cosmic rays cause them to cross the boundary and enter the heliosphere. These particles gyrate around the IMF but the presence of irregularities in the IMF scatters them away from a regular gyro motion. Also these IMF irregularities impact the convection of charged particles by mediating the interaction of the solar wind with the incoming cosmic rays. The overall impact of this phenomena is diffusion and convection of the particles from the heliospheric boundary towards the Sun. However, this diffusive motion of particles is influenced by the gradient and curvature drifts in the IMF [1–3].

The solar modulation in the heliosphere results in streaming of particles that produces an anisotropy in the flux of galactic cosmic rays. This streaming may be decomposed into two major components, first one in the ecliptic plane and the second perpendicular to this plane. The galactic cosmic rays entering the Earth's atmosphere produce a number of secondary particles. However, among the secondary particles, neutrons and muons reach the ground level and may be studied by the detectors placed on the surface of the Earth. The streaming in the ecliptic plane can be recorded by ground based detectors as a diurnal variation in the counting rate, super-

* Corresponding author at: Tata Institute of Fundamental Research, Mumbai 400 005, India.
E-mail address: gupta@grapes.tifr.res.in (S.K. Gupta).

http://dx.doi.org/10.1016/j.astropartphys.2014.07.003
0927-6505/

posed on a larger isotropic component. The streaming of primary cosmic rays responsible for this variation is known as the Solar Diurnal Anisotropy [1]. On the other hand, the streaming perpendicular to the ecliptic plane in the north–south direction is observed as a sidereal diurnal variation by the ground based detectors [4].

Several studies using the muon telescopes have shown the presence of such a sidereal variation along the north–south direction. At energies below 100 GeV, the sidereal diurnal variations caused by the solar modulation of the galactic cosmic rays in the heliosphere become dominant. This variation results from the streaming of cosmic rays $\mathbf{B} \times \mathbf{G}_r$ perpendicular to the plane of the ecliptic along the north–south direction, here $\mathbf{B}$ is the IMF and $\mathbf{G}_r$ the radial density gradient of the cosmic rays in the heliosphere [4]. This streaming results in generation of a diurnal variation in sidereal time, due to the tilt of the rotation axis of Earth relative to the plane of the ecliptic. Therefore, a muon telescope observes a maximum counting rate at 18 h local sidereal time, if the streaming is downward (north–south) and at 6 h local sidereal time if the streaming is upward (south–north). Since $\mathbf{G}_r$ points radially outward this streaming process reverses its direction whenever the polarity of the IMF changes. The region of the heliosphere where the IMF is directed toward the Sun, is called the Toward or TW sector, and the streaming is downwards (north–south). Similarly, when the IMF is directed away from the Sun, it is termed the Away or AW sector and the streaming is upwards (south–north). Therefore, the muon telescopes located in the northern hemisphere of the Earth detect a maximum rate at 6 h in the AW sectors and at 18 h in the TW sectors, in local sidereal time. This streaming as mentioned earlier is referred as the Swinson flow. The Swinson flow can be nearly eliminated when averaged over a year provided the AW and the TW sectors are of similar duration. On the other hand, the characteristics of the Swinson flow may be extracted by taking the difference of the mean variations in the AW and TW sectors because the Swinson flow is north–south asymmetric in the ecliptic plane [5].

A spurious sidereal diurnal variation could also be generated by seasonal variation of the solar diurnal anisotropy as explained below. The line of sight of a muon telescope towards the Sun undergoes a systematic annual change due to the orbital motion of Earth, resulting in an annual modulation of the solar diurnal variation. This modulation may be resolved into a sidereal and an anti-sidereal diurnal component of equal amplitude [6,7]. However, this spurious variation can be easily eliminated by using the anti-sidereal diurnal variation mentioned above [8]. After eliminating this spurious effect, the surviving effect contains the Swinson flow and the genuine sidereal diurnal anisotropy. The Swinson flow is sensitive to the polarity of the IMF in the vicinity of the Earth, a linear combination of the measurements from the TW and AW sectors may be exploited to extract the Swinson flow from the measured sidereal diurnal variation as detailed later in this work. Since the Swinson flow is produced by the solar modulation, it may be used to obtain the radial density gradient of the charged cosmic rays [2,9,10].

Various anisotropic phenomena involving the transport of the cosmic rays in the heliosphere, also known as the solar modulation were theoretically investigated by Parker and others [1]. These phenomena are well described by the diffusion–convection model. In the present work, the data for a relatively long duration of six years were analyzed. This long duration is expected to result in the reduction of the effects of the time dependent solar activity. Thus, a simple diffusion–convection equation without any time dependent terms as expressed by the following equation was used,

$$\mathbf{V_{sw}}\, n + \kappa \nabla n = 0 \tag{1}$$

where, n and ∇n, are the density and radial density gradient of cosmic rays, κ and $\mathbf{V_{sw}}$ represent the diffusion coefficient and the velocity of the solar wind, respectively. Here, the radial density gradient $\mathbf{G_r}$ and n are related by $\mathbf{G_r} = \nabla n/n$. The diffusion coefficient may be used to obtain the value of the mean free path of the cosmic rays in the heliosphere because these two parameters are two equivalent descriptions of the same phenomenon. Although, Parker and others had originally used the diffusion–convection framework to describe the dynamics of cosmic rays inside the solar system, it was subsequently employed by several workers to study the acceleration of charged particles in the shock waves produced by supernova explosions ([11] and references contained therein). This clearly indicated that the experimental studies using the framework of diffusion–convection model could be an effective tool to probe the mechanisms of the cosmic ray acceleration in our galaxy besides the solar system.

A number of early measurements were made to experimentally determine different parameters in the Parker equation. However, most of these measurements were made using relatively low energy cosmic rays observed by the ground based neutron monitors at energies $\lesssim$10 GeV or by the satellite based detectors at even lower energies [10]. The GRAPES-3 experiment [14] contains a large area (560 m^2) tracking muon telescope [15] that allowed even a small variation in the muon flux to be measured with high statistical precision. In the present work, an attempt was made to experimentally measure the radial density gradient of the galactic cosmic rays, without recourse to Monte Carlo simulations, and by using higher energy (77 GeV) galactic cosmic rays. Here, it needs to be emphasized that only the GRAPES-3 muon data were used in the present study for estimating the density gradient of galactic cosmic rays near the Earth. The use of data from an experiment located at a single geographic location avoided the systematic uncertainties that are normally associated with the use of data from multiple locations due to varying physical conditions and different characteristics of detectors used.

2. GRAPES-3 experimental setup

The GRAPES-3 experiment was set up at Ooty (11.4°N latitude, 76.7°E longitude, and 2200 m altitude) in south India. The GRAPES-3 experiment consists of two major components, the first component is an extensive air shower array of compact configuration with an inter-detector separation of 8 m between the adjacent plastic scintillator detectors, each 1 m^2 in area [12,13]. These detectors were deployed in a symmetric hexagonal geometry. At present, the array is being operated with about 400 detectors. The array was designed to study the primary cosmic rays from 10 TeV to 100 PeV and to make precision measurement of their energy spectrum and composition [14,16].

The second major component of the GRAPES-3 experiment is a large area tracking muon telescope that is used to measure the muon content of the cosmic ray showers [15]. This information is critically important in determining the composition of the primary cosmic rays [17]. This unique instrument was also used to measure the variation of the cosmic radiation due to the solar activity [18–20]. The muon telescope is capable of providing a high statistics, directional measurement of the muons. The GRAPES-3 muon telescope consists of a total of 16 individual modules, each of them with an area of 35 m^2. The basic element of the muon telescope is the proportional counter (PRC) fabricated from a rugged 600 cm long seamless steel pipe with 2.3 mm thick wall and a square cross-section of 10×10 cm^2. A module of sensitive area 35 m^2 consists of 232 PRCs arranged in four layers of 58 PRCs each, with alternate layers aligned in mutually orthogonal directions as shown schematically in Fig. 1. Two successive layers of the PRCs are separated by a 15 cm thick reinforced cement concrete layer assembled from blocks, each 60 cm $\times$ 60 cm $\times$ 15 cm in size. The four-layer PRC configuration of the muon module allowed

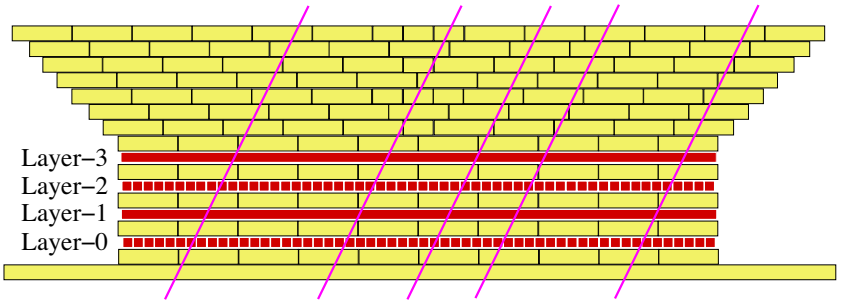

Fig. 1. A schematic of the 4-layer tracking muon telescope module with 58 PRCs per layer. Four layers of PRCs labeled Layer-0, Layer-1, ... embedded in concrete. Inclined lines indicate five parallel muons.

reconstruction of each muon track in two mutually orthogonal planes. The vertical separation of the two PRC layers in the same projection plane was ∼50 cm allowing measurement of the muon track direction with an accuracy of $\lesssim 6^\circ$ in each projected plane. The four layers of PRCs, namely, layers-0, 1, 2, and 3 in mutually orthogonal directions were interleaved with absorber concrete blocks that are clearly visible Fig. 1. Also shown in Fig. 1 are five tracks of inclined parallel muons.

To achieve an energy threshold of 1 GeV for vertical muons, an absorber of thickness ∼550 g cm^{-2} in the form of concrete blocks was used as shown schematically in Fig. 1. The concrete blocks were arranged in the form of an inverted pyramid to shield the PRCs with absorber coverage up to 45° for incident muons. Consequently, the muon telescope had an energy threshold of sec (θ) GeV for the muons incident at a zenith angle of θ. As shown in Fig. 2, the arrival direction of a muon was determined for each triggered PRC in the lower layer and binned into 13 directions based on the specific location of the PRC triggered in the upper layer from among the 13 PRCs, one directly above (central PRC) and six each on either side of the central PRC. This directional binning was carried out in each of the two orthogonal projection planes, thereby generating a map of 13 × 13 = 169 solid-angle directions of the muons as shown in Fig. 3. The contents of the 169 directions were recorded once every 10 s, thereby generating a continuous record of the directional flux of muons in the sky.

However, to obtain a higher statistical precision, the 169 directions were combined into nine coarse directions as shown schematically in Fig. 3. This was done by combining either a set of 3 × 5 or 5 × 5 solid-angle directions with the exception of the vertical direction, where the central 3 × 3 solid-angle directions were

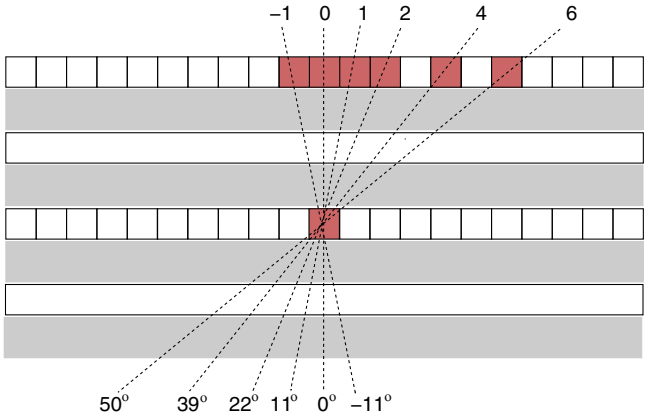

Fig. 2. Schematic view of muon arrival angle selection based on triggered PRCs, one in the lower and one from among the 13 PRCs in the upper layer. Triggered PRCs shown as filled squares.

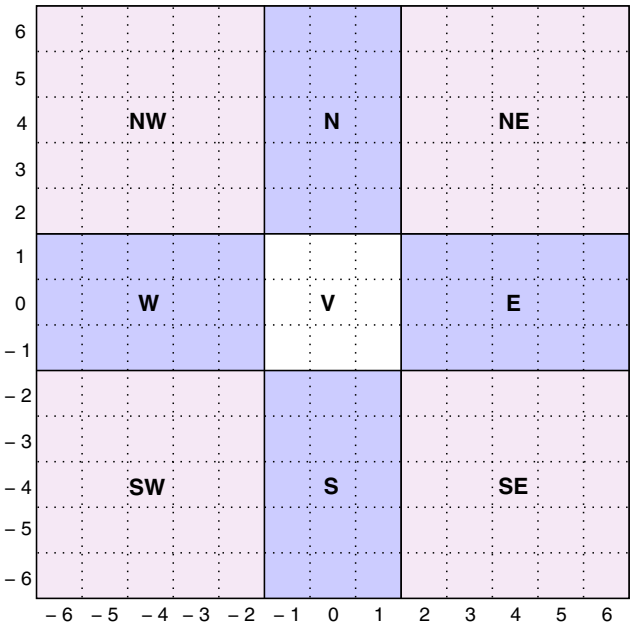

Fig. 3. A schematic of 169 muon directions that were subsequently combined into nine coarse directions. First, 3 × 3 vertical direction V, four 3 × 5 central (N,E,W,S), and four 5 × 5 outer directions (NE,SE,SW,NW).

combined. This specific combination scheme resulted in a relatively similar solid-angle coverage for these nine coarse directions. This choice of the angular segmentation also reduced the dissimilarity in the number of muons recorded in each coarse direction, because of the comparatively larger flux of muons for the near central directions (N,E,W,S) when compared to the outer directions (NE,SE,NW,SW). The cutoff rigidity at Ooty was 17 GV in the vertical direction and it varied from 14 to 32 GV across the field of view (FOV) of the muon telescope. However, in the present work only the data from the E, V, and W directions were utilized.

3. Data analysis

3.1. Data cuts

As described earlier, the one-dimensional Parker convection–diffusion framework provides a relationship among the radial density gradient of the cosmic rays, the solar wind velocity ($\mathbf{V_{sw}}$), and the cosmic ray diffusion coefficient (κ). The GRAPES-3 experiment detected the muons of energy above 1 GeV, that correspond to a median energy of ∼66 GeV for the primary cosmic ray protons in the vertical direction and varied from a low of 64 GeV–92 GeV across the FOV of the GRAPES-3 muon telescope. The median

energy of all primary cosmic ray protons within the FOV of muon telescope was ~77 GeV. These values of the median proton energies were estimated with the help of the international geomagnetic reference field model (IGRF-11) of the geomagnetic field [21] and Monte Carlo simulations using the CORSIKA package [22]. Thus the measurements using the GRAPES-3 data described below correspond to a median rigidity of ~77 GV. Since the GRAPES-3 tracking muon telescope recorded about 4×10^9 muons every day or $\sim 1.5 \times 10^{12}$ muons per year, it thus provided a directional survey of the sky with exceptional statistical precision.

The solar diurnal variation at a rigidity of ~77 GV was studied from the measured flux of muons by adopting the following procedure. The muon data for intervals of one hour were individually segregated for each of the nine directions after correcting for the dead-time. Next, a two step process was employed to effectively identify and remove the gaps and fast transients present in the data. This was necessary because such transients and data gaps had the potential to disturb the measurement of the Swinson flow that varies slowly with time. The root mean square (rms) deviation labeled σ_1 for each of the nine directions were calculated. For each direction the hourly data set corresponding to a deviation $\geq 10\sigma_1$ were rejected as abnormal. This procedure was repeated a second time for the data after the first step to recalculate the mean and the rms (σ_2). Next, the data with a deviation of $\geq 5\sigma_2$ were also rejected. The implementation of this rigorous two step cut eliminated poor quality data segments that included data gaps, gain variations, and the transient phenomena such as the Forbush decrease events of magnitude larger than 3%. Thereafter, the hourly muon rate for each direction was corrected by using the pressure coefficients for the corresponding direction for variation in the atmospheric pressure. Finally, the hourly muon rates were expressed as fractional changes (in %) from the mean of the data for the six year period (2000–05) for each of the nine directions.

After completion of the above quality cuts, short-term transients were also removed from the data while retaining the long-term variations including the 27-day, the seasonal (annual) and the 11-year solar effects and other short-term periodic behaviors such as the sidereal and solar diurnal variations. Next, to probe the short-term periodic variations, it became essential to filter out the slower long-term variations listed above. The effects of long-term variation were removed by devising an indirect high-pass filter. The high-pass filter was implemented by the following procedure. A running mean $H(\text{low})_i$ of the hourly muon rates h_i was calculated for each hour by taking the data of 12 h on either side of a given hour for each of the nine directions. This running mean provided an effective low-pass filter $H(\text{low})_i$ of the hourly rates. Then, the running mean $H(\text{low})_i$ was subtracted from the corresponding observed hourly rate h_i to obtain the hourly high-pass data $H(\text{high})_i$ for the nine directions. For further analysis of the solar and sidereal diurnal variations, we selected only the days that contained data for each of the 24 h without any gap.

In order to remove the residual effects of the transient phenomena such as a Forbush decrease event, the calender days with significant transient activity were identified by using the Kiel neutron monitor data [23]. Due to a lower cutoff rigidity, the Kiel neutron monitor recorded a large amplitude even for Forbush decrease events of relatively small magnitude and thus could be used to identify such events. The following criteria were used to identify the days of transient activity, (a) daily rate N_i for the ith day was compared with the mean daily rate N_M for the previous three days. Here, the rates N_i and N_M were expressed in %. If the value of $(N_M - N_i) = \Delta N$ exceeded 4% then the data for the ith day for all nine directions were attributed to be influenced by a transient phenomena and rejected, (b) The days following the ith day defined above were also attributed to the recovery phase of the transient phenomena. If the deviation from N_M of the neutron monitor rates $N_{i+1}, N_{i+2}, \ldots$ for the following days exceeded $0.3 \times \Delta N$, then the data for $(i+1)$th, $(i+2)$th, ... were deemed to lie in the recovery phase and rejected.

3.2. East–West method

The GRAPES-3 muon data were influenced by several effects including those induced by the atmospheric pressure and temperature. The variation in muon rates due to pressure changes were corrected as described earlier. However, it was not possible to correct for the effects of temperature and other unknown factors. Therefore, we adopted a powerful technique proposed by Kolhörster and others [24–26], which is capable of eliminating the effects listed above. This East–West method was implemented as described below.

The variation in the intrinsic anisotropy in space may be calculated by using the measurements from the E and W directions and τ, where τ is the time offset between E and W directions as shown below,

$$\Delta I = I(t + \Delta t) - I(t) = I(t + \tau/2) - I(t - \tau/2) = N_{\text{E}}(t) - N_{\text{W}}(t) \quad (2)$$

If the intrinsic anisotropy $I(t)$ in space is superposed on an isotropic component B and a common time dependent variation $C(t)$ of atmospheric origin, then the time variation recorded along the V, E, and the W directions, $N_{\text{V}}(t)$, $N_{\text{E}}(t)$, and $N_{\text{W}}(t)$, respectively, may be written as,

$$N_{\text{V}}(t) = I(t) + B + C(t) \quad (3)$$
$$N_{\text{E}}(t) = I(t + \tau/2) + B + C(t) \quad (4)$$
$$N_{\text{W}}(t) = I(t - \tau/2) + B + C(t) \quad (5)$$
$$N_{\text{E}}(t) - N_{\text{W}}(t) = I(t + \tau/2) - I(t - \tau/2) \quad (6)$$

By summing the difference $N_{\text{E}}(t) - N_{\text{W}}(t)$ obtained from the GRAPES-3 observations, the time independent anisotropy in space was reconstructed using the East–West (E–W) method as detailed below. However, one needed to experimentally measure the time offset τ corresponding to the hour angle difference between the E and W directions. The hourly muon rates expressed as percent deviation from the six year mean for E, and W directions for all six years of data were each folded modulo 24 h. The time offset τ due to the hour angle difference between E and W was precisely calculated by using the cross correlation of the muon rates from these two directions. The result of this correlation study is shown in Fig. 4. The maximum correlation between E and W was obtained for an offset

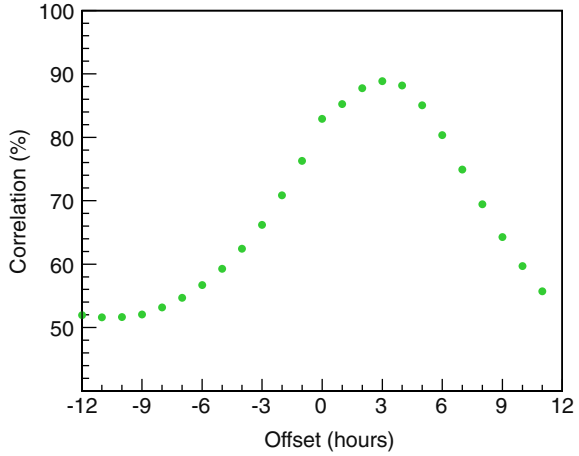

Fig. 4. Correlation between E and W as a function of time offset (h). Maximum correlation of 89% observed for offset of 3 h consistent with the hour angle of 3 h between E and W directions.

of $\tau = 3$ h, exactly as expected from the geometry of the GRAPES-3 muon telescope.

The hourly muon rates expressed as percent deviation from the six year mean for E, W, and V, directions after folding modulo 24 h for six year interval are shown in Fig. 5(a)–(c), respectively. The plot shown in Fig. 5(d) was obtained by using the E–W method as described below. This was achieved by using the offset of 3 h obtained earlier and the hourly rate for the E and W directions. Thereafter, the expected hourly time variation for the V direction was obtained as shown in Fig. 5(d).

3.3. Data classification by IMF

Next, we describe the methodology followed in identifying the days that were characterized by the IMF oriented either toward (labeled 'TW') or away ('AW') from the Sun, respectively. The geocentric solar ecliptic (GSE) coordinate system with the Earth at the origin was used. The positive X-axis was defined along the line joining the Earth to the Sun, and the negative Y-axis was tangent to the orbit of the Earth along the direction of its motion. The positive Z-axis was along the north ecliptic pole forming a right-handed Cartesian coordinate system. The magnetic field data showed that the magnitude of the 'z' component of IMF, B_z was much smaller than the other two components, namely, B_x and B_y and hence only the latter two components were used [27]. A running mean of the hourly values of B_x and B_y were calculated over an interval of 72 h centered on the current hour and tabulated into four categories as listed in Table 1. As mentioned earlier, the median energy of the primary protons responsible for the muons detected in the GRAPES-3 muon telescope was ~77 GeV. The choice of 72 h was dictated by the fact that the Larmor radius of a 77 GeV proton is ~0.36 AU in an observed mean IMF of 4.7 nT. For a typical velocity of 400 km/s, the solar wind takes about 36 h to travel a distance of 0.36 AU. Thus a 72 h interval centered on the hour in question allowed a reasonable estimate of the effective IMF to be obtained. Using the above procedure the running mean of the IMF components were calculated and based on the sign of B_x and B_y, the data were assigned to one of the four categories listed in Table 1 for each of the 24 h in a calender day.

If the IMF data for each hour in a day fell exclusively into either the AW or the TW category, then that day was selected for further analysis. Based on the complete days collected during 2000–05, about 79% of days fell into either AW or TW categories, and the remaining 21% into the mixed category and hence were excluded from further analysis as mentioned in Table 2.

It was difficult to directly extract the sidereal diurnal variation because its amplitude was about an order of magnitude smaller than the solar diurnal variation. Therefore, we indirectly estimated the amplitude of the sidereal diurnal variation as explained below. Since the sidereal and the solar years synchronize once in a year, due care was taken to ensure that the data for the whole years were used to extract these anisotropies. If the solar diurnal anisotropy had a constant amplitude, then the data analyzed for the sidereal diurnal anisotropy for a complete year would wipe out the solar diurnal anisotropy. However, the small inclination angle of 7.3° between the solar equatorial plane and the plane of the ecliptic introduced a seasonal variation which manifested as a sidereal and an anti-sidereal variation of equal amplitude. In addition, there might have been other causes of seasonal variation that could mimic a sidereal and an anti-sidereal variation. Therefore, an analysis strategy was devised to identify and largely eliminate these seasonal effects. Since there were gaps in the data due to rejection of the days when the IMF did not fall into AW or TW category, it was important to use a method that would not have introduced any side bands.

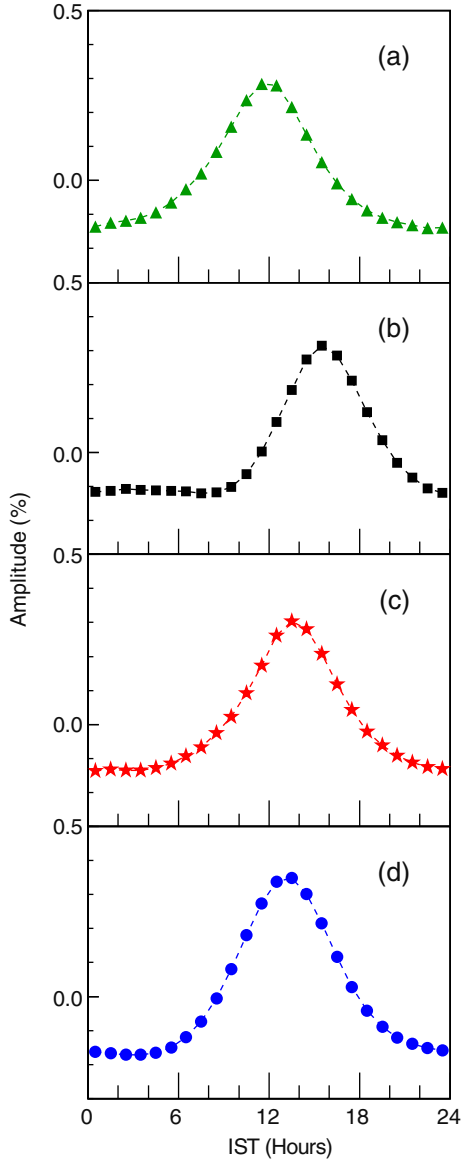

Fig. 5. Percent deviation from hourly mean muon rate for 2000–05 data for, (a) E, (b) W, (c) V, and (d) V_{EW}.

Table 1
Category of IMF directions.

#	B_x	B_y	Type	Action
1	<0	<0	Mixed	Reject
2	⩽0	⩾0	Away	Accept
3	⩾0	⩽0	Toward	Accept
4	>0	>0	Mixed	Reject

Table 2
Data categories.

Class	Days
Total days (2000–05)	2192
Full days (All)	2015
Full days (TW)	784
Full days (AW)	810
Full days (Mix)	421

The data for a given calender month, say January 2001 were sorted into two groups labeled, Jan01AW and Jan01TW containing the data corresponding to AW and TW categories, respectively. Next, the mean of the data for each hour for all days present in Jan01AW were calculated to extract the variation in 1 h intervals for this category. The same exercise was repeated for the Jan01TW data. These monthly data pairs were then used for further analysis. The monthly data for six years (72 sets each) were individually combined to yield the TW and AW profiles. The mean of the TW and AW profiles largely caused by the solar diurnal anisotropy for the period 2000–05 are shown in Fig. 6(a) and in Fig. 6(b), respectively. The height of the peaks for the TW and AW categories as seen from Fig. 6(a) and (b) are very similar clearly indicating that the polarity of the IMF had very little effect on the amplitude of the solar diurnal anisotropy.

In principle, the TW and the AW data might have contained the contributions from the IMF polarity independent effects such as the solar diurnal anisotropy and possible IMF polarity dependent effects. The sum (TW+AW)/2 cancels out the IMF polarity dependent effects, while retaining the IMF polarity independent solar diurnal anisotropy. The mean solar diurnal variation represented by (TW+AW)/2 for the period 2000–05 when calculated was nearly identical to the plots shown in Fig. 6(a) and (b). Due to their similar profiles the data for the AW and the TW categories were combined and the amplitude of the solar diurnal variation was estimated to be ~0.3% which peaked at 13 h Indian Standard Time (IST) [28]. This corresponded to an asymptotic direction of 16 h IST. Similarly, the quantity (TW−AW)/2 canceled out the IMF polarity independent solar diurnal anisotropy, while retaining the IMF polarity dependent effects. However, this exercise did not show a clear indication of an IMF dependent anisotropy in the GRAPES-3 data. A more sensitive analysis is needed to probe the potential presence of such an IMF polarity dependent solar anisotropy.

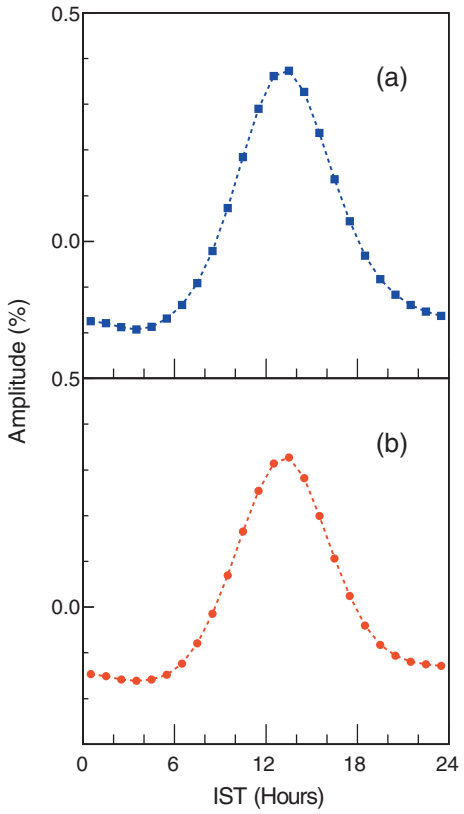

Fig. 6. Muon rate variation (%) due to solar diurnal anisotropy (2000–05) for, (a) TW, (b) AW categories.

By employing the E–W method outlined earlier, the variation in the TW and the AW sectors were obtained by folding the monthly data modulo the solar day. Next, the quantity (TW−AW)/2, which is IMF polarity sensitive was calculated for each month. To estimate the sidereal anisotropy the (TW−AW)/2 data from successive months were shifted backwards by 2 h relative to the previous month, to synchronize the data to the sidereal clock. The variation of (TW−AW)/2 for the period 2000–05 is shown in Fig. 7(a) which represents the effect of the IMF polarity dependent sidereal anisotropy as measured using the GRAPES-3 muon data.

The presence of the seasonal effects on the solar diurnal variation through an interference introduces both a sidereal and an anti-sidereal variation of equal amplitude. The procedure outlined in the previous paragraph when repeated by shifting the data forward by 2 h synchronized the data to an anti-sidereal clock, thus canceling the sidereal variations while retaining the contribution of the seasonal effects as shown in Fig. 7(b). In view of a relatively small amplitude the contribution of the seasonal effects on the observed sidereal variation is also expected to be very small. Next, the anti-sidereal contribution from Fig. 7(b) was used to correct the measured sidereal variation shown in Fig. 7(a) by using the prescription of Nagashima and coworkers [8] to obtain the correct amplitude of sidereal variation. This variation representing the Swinson flow is shown in Fig. 7(c). The fact that the amplitude of the Swinson flow before and after the correction was nearly same is due to a very small amplitude of the seasonal correction displayed in Fig. 7(b).

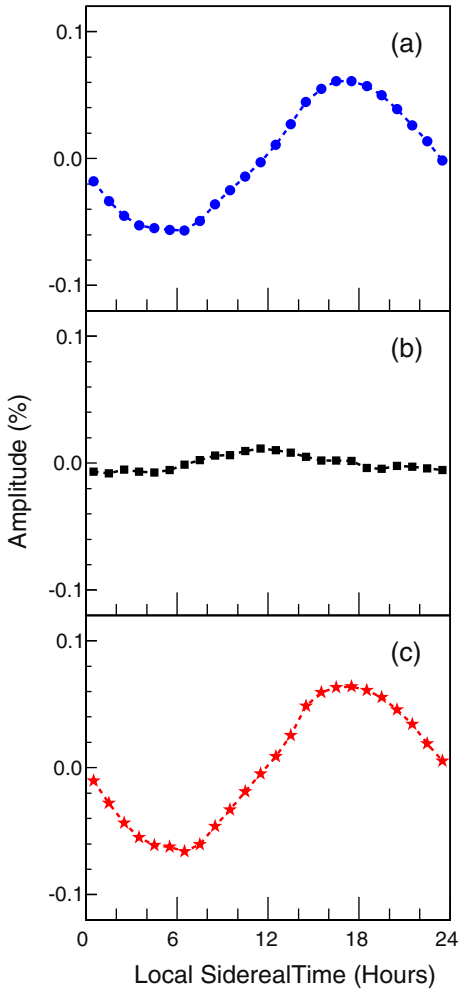

Fig. 7. Muon rate variation (%) due to sidereal diurnal anisotropy for 2000–05, (a) (TW−AW)/2, (b) anti-sidereal contribution (c) corrected (TW−AW)/2

The variation due to the Swinson flow represented by the corrected (TW−AW)/2 shown on Fig. 7(c) displays a minimum at ∼6 h sidereal time. This may be understood with the help of a schematic of the interplanetary medium that includes the Sun and the Earth as shown in Fig. 8. The gradient in the radial density of the cosmic rays results in radially inward diffusion of cosmic rays. When the IMF points toward the Sun as shown in Fig. 8(a), the Lorentz force exerted on the cosmic rays diffusing inward induces a north–south flow, perpendicular to the ecliptic plane that displays a minimum at ∼6 h sidereal time and a maximum at ∼18 h as seen from Fig. 8(a). However, when the IMF points away from the Sun then the resultant flow displays a maximum at ∼6 h sidereal time and a minimum at ∼18 h as shown in Fig. 8(b). Therefore, the parameter (TW−AW)/2 provides a more precise measure of this north–south TW flow by eliminating the common sources of errors caused other phenomena. The symmetry of the plot in Fig. 7(c) implies that the Swinson flow along both, the north to south and the south to north directions had nearly the same magnitude. Since the variation shown in Fig. 7(c) displayed a periodic behavior it was decided to perform a fit by using sine and cosine terms as follows. The data for each hour as t_i, and corresponding amplitude and error as N_i, and σ_i, where $i = 1, 2, 3, \ldots n$ $(n = 24)$. The following function $F(t_i)$ was fitted to the data by least squares method,

$$F(t_i) = a\cos\left(2\pi\frac{t_i}{24}\right) + b\sin\left(2\pi\frac{t_i}{24}\right) \tag{7}$$

where $n = 24$ is the number of data points and the values a and b were determined as described below. The weighted sum (S) of the squares of residuals (Δ_i) is expressed as,

$$S = \sum_{i=1}^{n}\frac{\Delta_i^2}{\sigma_i^2}\Big/\sum_{i=1}^{n}\frac{1}{\sigma_i^2} \tag{8}$$

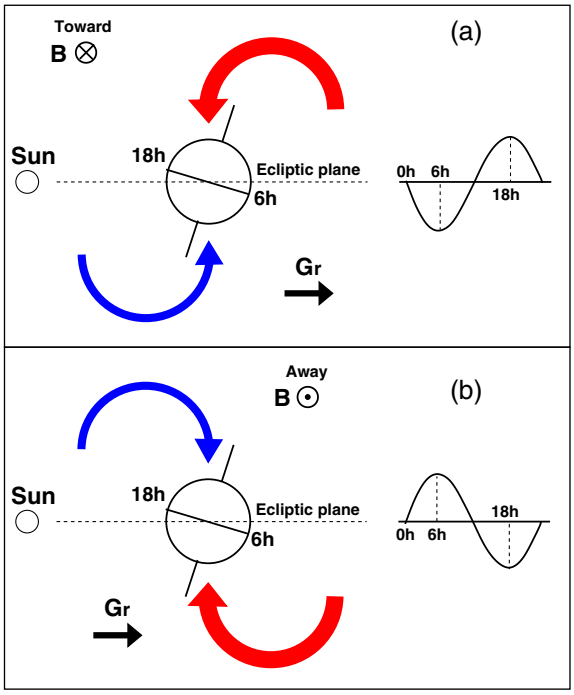

Fig. 8. Schematic of Swinson flow at Earth indicated by colored arrows due to diffusion of cosmic rays in IMF. Curved thick red arrow indicates excess flow and blue thin arrow deficit flow. IMF relative to Sun in, (a) TW sector, sinusoidal flow with maximum at 18 h, (b) Away sector, sinusoidal flow with maximum at 6 h. (TW−AW)/2 removed common systematic effects and yielded actual TW flow.

Since in the present case variation in the value of σ_i was negligibly small, the above calculation was carried out with a constant value of $\sigma_i = \sigma$ for all i as given below,

$$S = \sum_{i=1}^{n}\Delta_i^2 = \sum_{i=1}^{n}\left\{N_i - a\cos\left(2\pi\frac{t_i}{24}\right) - b\sin\left(2\pi\frac{t_i}{24}\right)\right\}^2 \tag{9}$$

By minimizing the quantity S with respect to a and b, one obtains,

$$a = -0.0050 \pm 0.0052\% \tag{10}$$
$$b = -0.0642 \pm 0.0052\% \tag{11}$$

and this fit yielded $\chi^2 = 0.468$ for a total of $(n-2) = 22$ degrees of freedom which is too small a value to be realistic. Such a small value of χ^2 clearly indicated the presence of a large systematic variation, and therefore, the true error was estimated from the sum of square of the deviation S of the data points from the function listed in Eq. (7). This was implemented by minimizing the rms deviation of the data points from the function described in Eq. (7). A proper propagation of the errors led to the following estimate of the rms deviation σ,

$$\sigma = \sqrt{\frac{1}{n-2}\sum_{i=1}^{n}\Delta_i^2} \tag{12}$$

solution of the above equation yields the value of σ to be,

$$\sigma = \sqrt{\frac{0.00014694}{(24-2)}}\% = 0.0026\% \tag{13}$$

This value of σ = 0.0026% is approximately seven times smaller than the value of 0.018% estimated from the rms deviation of hourly values for 72 months of data. Clearly, the Swinson flow despite showing a sizable variation over a time scale of six years had a remarkable underlying stability that had manifested in a rather stable profile characterized by a small value of $\sigma = 0.0026\%$. By incorporating this new value of σ the errors in amplitudes a and b were estimated to be,

$$a = -0.0050 \pm 0.0008\% \tag{14}$$
$$b = -0.0642 \pm 0.0008\% \tag{15}$$

From these two parameters the actual amplitude A and the phase ϕ was found to be,

$$A = 0.0644 \pm 0.0008\% \tag{16}$$
$$\psi = 17.70 \pm 0.05\ \text{h} \tag{17}$$

Thus the amplitude of the Swinson flow as measured by GRAPES-3 as shown in Fig. 7(c) was $(0.0644 \pm 0.0008)\%$ with a phase of (17.70 ± 0.05) h, which was close, but not identical to its expected value of 18 h. The difference in the expected and measured phases of (18 ± 3) min had a significance of nearly 6σ.

In the present work the direction from south to north, perpendicular to the ecliptic plane was referred as the upward and the one from north to south as the downward direction. The magnitude of the Swinson flow was estimated as explained in the following. It was assumed that the Swinson flow caused an anisotropy of magnitude $\xi\%$, perpendicular to the ecliptic plane along the downward direction. This angular dependence may be expressed as $1 + \xi\cos\theta$, where θ is the angle relative to the perpendicular described above. A muon telescope on Earth would observe this anisotropy as a sidereal diurnal variation and for a location on the equator an amplitude of $\xi\sin\phi$ would be observed with a maximum at a sidereal time of 18 h, where ϕ is the angle between the equatorial and ecliptic planes. However, a telescope located at a latitude λ in the northern hemisphere would observe an amplitude of $\xi\sin\phi\cos\lambda$ with a maximum also at a sidereal time of 18 h.

The angle between the upward perpendicular to the ecliptic and the vertical direction at a latitude λ on Earth may be expressed as $\theta_1 = \pi/2 - \lambda - \phi$ at a sidereal time of 18 h and $\theta_2 = \pi/2 - \lambda + \phi$ at 6 h. Therefore, a telescope located at a latitude λ in the northern hemisphere observing the cosmic rays in the vertical direction would observe the difference between the maximum and minimum of the anisotropy, $\xi(\cos\theta_1 - \cos\theta_2) = \xi\{\sin(\lambda+\phi) - \sin(\lambda-\phi)\} = 2\xi\cos\lambda\sin\phi$. Thus the magnitude of the anisotropy ξ (%) may be calculated from the amplitude A (%) estimated earlier directly from data,

$$\xi = \frac{A}{\cos\lambda\,\sin\phi} \tag{18}$$

By substituting the values λ and ϕ in the above equation,

$$A = 0.0644 \pm 0.0008\% \tag{19}$$

$$\lambda = 11.4^{\circ} \tag{20}$$

$$\phi = 23.5^{\circ} \tag{21}$$

The magnitude of the anisotropy caused by Swinson flow was obtained,

$$\xi = 0.1648 \pm 0.0020\% \tag{22}$$

4. Discussion

The large area GRAPES-3 tracking muon detector allowed measurement of the flux of >1 GeV muons along nine directions labeled NE, N, NW, E, V, W, SE, S, SW, each with a solid angle coverage of ~0.23 sr. The muons were detected at a rate of 1.8×10^8 h^{-1} enabling small variations in its flux to be reliably measured. A two step quality cut was imposed on the muon data to remove the data that had gaps, gain variation of the proportional counters, and was influenced by transient phenomena such as the Forbush decrease events etc. Despite these stringent cuts only 177 d (8%) out of 2192 d during the six years (2000–05) were rejected. By the use of the powerful E–W method, we could largely eliminate contributions due to various systematic effects including the ones of atmospheric origin, and reconstruct the actual time variation along the V direction. This variation represented the solar diurnal anisotropy that peaked at 13 h IST locally and 16 h IST asymptotically.

Using the IMF components B_x, B_y, B_z [27], the orientation of the IMF with respect to Sun was determined every hour. Depending on the orientation of the IMF being either toward (TW) or away (AW) from the Sun during a given day, the data for that day were accordingly classified as belonging to the TW or AW category. However, during the 24 h in a day when the orientation of the IMF was not exclusively TW or AW, then that day was classified as a mixed day and the data for such days were rejected. A total of 421 out of 2015 d fell into the mixed category, thereby resulting in a further rejection of about 21% of the data as listed in Table 2. Finally, 784 (TW) and 810 (AW) for a total of 1594 d out of 2015 d survived the final cuts. This data set has formed the base for the analysis presented here.

The difficulties in directly extracting the sidereal diurnal variation in the GRAPES-3 data in the presence of various atmospheric effects and a much larger solar diurnal variation were overcome by eliminating these effects using the E–W technique. Since the sidereal and solar years synchronize once in a year the data for integral number of years were used to extract the sidereal anisotropy. The equal amplitude sidereal and anti-sidereal variations produced by various seasonal effects were used to eliminate those seasonal effects. The data were carefully examined to ensure that the gaps in the data due to rejection of the days when the IMF was in the mixed category did not result in the introduction of new periodic variations.

The daily data from each calender month were subdivided into two groups corresponding to the AW and TW categories. Thereafter, the hourly rate for the days in a given month were used to calculate the variation for these two categories to generate monthly data for six years (72 sets each) for the TW and AW categories. The six year mean TW and AW profiles due to the solar diurnal anisotropy for the period 2000–05 displayed in Fig. 6(a) and (b) showed that the IMF polarity did not have a large effect on the amplitude of the solar diurnal anisotropy. The mean amplitude of the solar diurnal anisotropy for 2000–05 was estimated to be ~0.3%. The anisotropy as shown in Fig. 5(d) peaked at 13 h IST consistent with our measurements for 2006 using a different method [28].

Turning to the main objective of the present work, we next focused on the sidereal variation. The IMF polarity sensitive quantity (TW−AW)/2 was calculated for each month. For obtaining the sidereal variation, the (TW−AW)/2 data from successive months were shifted backwards by 2 h relative to the previous month, to synchronize the data to the sidereal clock and averaged. The variation of (TW−AW)/2 for the period 2000–05 thus obtained is shown in Fig. 7(a). The presence of the seasonal effects on the solar diurnal variation through interference introduces both a sidereal and an anti-sidereal variation of equal amplitude. The procedure outlined above was repeated for (TW−AW)/2 by shifting the data forward by 2 h to synchronize to the anti-sidereal clock. The anti-sidereal variation thus obtained represented the tiny amplitude of the seasonal effects as shown in Fig. 7(b). This variation was used to correct the observed sidereal variation. The corrected sidereal variation of (TW−AW)/2 is shown in Fig. 7(c), which was the IMF polarity dependent sidereal diurnal variation representing the projection of the Swinson flow along the direction V in the FOV of the GRAPES-3. The amplitude of the sidereal variation before and after the correction was nearly the same due to a very small amplitude of the correction as shown in Fig. 7(b).

The IMF polarity dependent sidereal diurnal variation shown on Fig. 7(c) displayed a minimum at ~6 h sidereal time, indicating the direction of the flow to be from south to north, perpendicular to the ecliptic plane. Similarly, the maximum at ~18 h sidereal time was indicative of the flow from north to south. Since the angle between the Swinson flow along the north–south (N–S) and the direction V in GRAPES-3 FOV is minimum at 18 h, the IMF polarity dependent sidereal diurnal variation projected along V was maximum. Similarly, the angle between S–N Swinson flow and V was minimum at 6 h, and the amplitude of the Swinson flow projected along V was maximum. The symmetry of the plot in Fig. 7(c) implied that the IMF polarity dependent sidereal diurnal variation along both the N–S and S–N directions was of nearly the same amplitude. Based on these measurements the amplitude of the Swinson flow was estimated to be (0.0644 ± 0.0008)%.

As described earlier, if the relative magnitude of the Swinson flow at a rigidity P was ξ%, the direction of this flow would be perpendicular to the ecliptic plane. The maximum intensity was observed if the muon telescope was pointing either along upstream or downstream of the Swinson flow. The rotation axis of the Earth is inclined by $\phi = 23.5^{\circ}$ relative to the ecliptic and the latitude of the GRAPES-3 site is $\lambda = 11.4^{\circ}$. Since the GRAPES-3 is located in the northern hemisphere, thus the maximum southward Swinson flow of $\xi\cos(\lambda+\phi)$ was expected to be observed at 18 h, and a minimum of $\xi\cos(\lambda-\phi)$ at 6 h sidereal time. Thus the amplitude of the IMF polarity dependent sidereal variation observed along V by the GRAPES-3 telescope is given by $\xi(\cos(\lambda+\phi) - \cos(\lambda-\phi))/2$ which equals $\xi\cos\lambda\sin\phi$. Using the observed value of $\xi\cos\lambda\sin\phi$ of (0.0644 ± 0.0008)% the relative

magnitude of the variation due to the Swinson flow was found to be $\xi = (0.1648 \pm 0.0020)\%$

The radial density gradient of the galactic cosmic rays near the Earth, based on our measurements may be estimated as described below. The density gradient $\mathbf{G_r}(P)$ of cosmic rays at a rigidity P may be formulated as follows,

$$-|\mathbf{G_r}(P)| \sim \frac{\xi(P)}{\rho \sin\chi} \tag{23}$$

Here, ρ is the gyro radius (Larmor radius) of the cosmic rays in the IMF, and χ the angle between the IMF and the direction of motion of the Earth and is expected to be $\sim 45°$. $\xi(P)$ represents the anisotropy along the north–south direction perpendicular to the ecliptic plane due to the Swinson flow. As explained earlier, the median rigidity of the cosmic rays responsible for the production of muons observed in the GRAPES-3 muon detector was $P = 77$ GV. From these parameters ρ was found to be 0.36 AU using the observed mean value of the IMF, $B = 4.7$ nT, measured near the Earth.

The radial density gradient of the cosmic rays at a rigidity of 77 GV was estimated to be 0.65% AU^{-1}, from these six years of observations with the GRAPES-3 experiment. The estimated density gradient from the GRAPES-3 data is comparable to the values reported by other workers [2,9]. For example, the parametrization given in [9] yielded a radial density gradient of 0.7% AU^{-1} for a rigidity of 77 GV. Similarly, the work in [2] implies a radial density gradient of <1.0% AU^{-1} at 100 GV.

5. Conclusion

The outward flow of solar wind results in a gradient in the radial density of galactic cosmic rays in the heliosphere due to the phenomenon of diffusion and convection. This gradient coupled with the interplanetary magnetic field results in a flow of charged particles termed the Swinson flow perpendicular to the ecliptic plane. The Swinson flow is manifested as a small anisotropy in sidereal time in the flux of cosmic rays and its amplitude and phase were measured using the GRAPES-3 tracking muon telescope data. The large area (560 m^2) of GRAPES-3 muon telescope resulted in the detection of $\sim 7.5 \times 10^{12}$ muons over the six year period during 2000–05. This high muon statistics was exploited to make a very high precision measurement of the amplitude of the Swinson flow, $\xi = (0.0644 \pm 0.0008)\%$ which is a nearly 80σ effect. The phase of the maximum flow was measured to be at a sidereal time of (17.70 ± 0.05) h. The phase of 17.7 h is close but different by 18 min from the expected value of 18 h. This difference of 18 min is small, yet is significant at the level of 6σ which is indicative of the precision of the GRAPES-3 measurement. The mean interplanetary magnetic field (IMF) was calculated to be 4.7 nT during the six year interval 2000–05. The median rigidity of the primary protons responsible for producing the muons detected by GRAPES-3 experiment was 77 GV. From these values of Swinson flow, mean IMF and median proton rigidity the cosmic ray radial density gradient was estimated to be 0.65% AU^{-1}. This value is consistent with the measurements reported by other groups.

Acknowledgment

We thank D.B. Arjunan, late S. Karthikeyan, S. Kingston, K. Manjunath, S. Murugapandian, B. Rajesh, C. Ravindran, V. Santhosh Kumar, R. Sureshkumar for their help in the operation, maintenance of the proportional counters and the associated electronics for the GRAPES-3 tracking muon telescope. We thank G.P. Francis, V. Jeyakumar, and K. Ramadass for their help in the repair and maintenance of various mechanical components in the muon telescope. The easy availability of the OMNI data from the GSFC/SPDF OMNIWeb interface at http://omniweb.gsfc.nasa.gov made it possible to determine the IMF direction which was a critical requirement of the data analysis. Use of the Kiel neutron monitor data was important for our analysis for which we are grateful to the Kiel group. This work was partially supported by the grants of the Solar Terrestrial Environment Laboratory of Nagoya University, the Institute for Cosmic Ray Research of University of Tokyo, Chubu University, and the National Astronomical Observatory of Japan.

References

[1] E.N. Parker, Phys. Rev. 110 (1958) 1445.
[2] D.L. Hall, M.L. Duldig, J.E. Humble, Space Sci. Rev. 78 (1996) 401.
[3] P.A. Isenberg, J.R. Jokipii, Astrophys. J. 234 (1979) 746.
[4] D.B. Swinson, J. Geophys. Res. 74 (1969) 5591; D.B. Swinson, J. Geophys. Res. 81 (1976) 2075.
[5] K. Munakata et al., J. Geophys. Res. 104 (1999) 2511.
[6] F.J.M. Farley, J.R. Storey, Proc. Phys. Soc. A 67 (1954) 996.
[7] K. Nagashima, H. Ueno, Rep. Ionos. Space Res. Jpn. 25 (1971) 212.
[8] K. Nagashima, R. Tatsuoka, S. Matsuzaki, Nuovo Cimento C 6 (1983) 550; R. Tatsuoka, K. Nagashima, Nuovo Cimento C 8 (1985) 320.
[9] S. Yasue, J. Geomagn. Geoelec. 32 (1980) 617.
[10] H. Moraal, Space Sci. Rev. 19 (1976) 845.
[11] W.I. Axford, Ap. J. Suppl. 90 (1994) 937.
[12] P.K. Mohanty et al., Astropart. Phys. 31 (2009) 24.
[13] P.K. Mohanty, S.R. Dugad, S.K. Gupta, Rev. Sci. Instrum. 83 (2012) 043301, http://dx.doi.org/10.1063/1.3698089.
[14] S.K. Gupta et al., Nucl. Instrum. Methods A 540 (2005) 311.
[15] Y. Hayashi et al., Nucl. Instrum. Methods A 545 (2005) 643.
[16] S.K. Gupta et al., Nucl. Phys. B Proc. Suppl. 196 (2009) 153.
[17] H. Tanaka et al., J. Phys. G: Nucl. Part. Phys. 39 (2012) 025201.
[18] T. Nonaka et al., Phys. Rev. D 74 (2006) 52003.
[19] P. Subramanian et al., Astron. Astrophys. 494 (2009) 1107.
[20] K.P. Arunbabu et al., Astron. Astrophys. 555 (2013) A139, http://dx.doi.org/10.1051/0004-6361/201220830.
[21] C.C. Finlay et al., Geophys. J. Int. 183 (2010) 1216.
[22] <http://www-ik.fzk.de/corsika>.
[23] <http://134.245.132.179/kiel/main.htm>.
[24] W. Kolhörster, Phys. Z. 42 (1941) 55.
[25] H. Alfvén, K.G. Malmfors, Arkiv. Mat. Astron. Fysik. 29A (1943) 24.
[26] H. Elliot, D.W.N. Dolbear, J. Atmos. Terr. Phys. 1 (1951) 205.
[27] J.H. King, N.E. Papitashvili, J. Geophys. Res. 110 (2004) A02209, http://dx.doi.org/10.1029/2004JA010804. <http://omniweb.gsfc.nasa.gov/html/omni2_doc.html> .
[28] P.K. Mohanty et al., Pramana J. Phys. 81 (2013) 343.